Vessel Orientation Constrained Quantitative Susceptibility Mapping (QSM) Reconstruction

-, -, and -

_
_
{--,--,--}@-.-

Abstract. QSM is used to estimate the underlying tissue magnetic susceptibility and oxygen saturation in veins. This paper presents vessel orientation as a new regularization term to improve the accuracy of l_1 regularized QSM reconstruction in cerebral veins. For that purpose, the vessel tree is first extracted from an initial QSM reconstruction. In a second step, the vascular geometric prior is incorporated through an orthogonality constraint into the QSM reconstruction. Using a multi-orientation QSM acquisition as gold standard, we show that the QSM reconstruction obtained with the vessel anatomy prior provides up to 40% RMSE reduction relative to the baseline l_1 regularizer approach. We also demonstrate in vivo OEF maps along venous veins based on segmentations from QSM. The utility of the proposed method is further supported by inclusion of a separate MRI venography scan to introduce more detailed vessel orientation information into the reconstruction, which provides significant improvement in vessel conspicuity.

Keywords: QSM, Susceptibility MRI, QSM reconstruction, vessel orientation constraint

1 Introduction

Susceptibility MRI provides exquisite contrast of the venous vasculature due to the presence of paramagnetic deoxyhemoglobin molecules in cerebral veins. Although susceptibility-weighted imaging has gained popularity due to its ability to depict the veins in clinical applications such as stroke [1] and traumatic brain injury [2], this method suffers from non-local and orientation-dependent effects that may preclude accurate identification of brain vessels.

As an alternative, vessel segmentation can be performed directly on QSM derived from MRI phase images [3, 4]. Because dipolar field patterns have been deconvolved during QSM reconstruction, segmentation of vasculature on QSM images is expected to outperform magnitude- or phase- based approaches. Automated vessel detection may also provide anatomical priors to improve quantification of brain physiology from QSM, including oxygen extraction fraction (OEF) in cerebral veins. Baseline OEF is an important physiological parameter for tissue health in normal brain function and many cerebrovascular diseases [5]. Reliable estimation of OEF depends on robust and accurate QSM reconstruction within venous structures.

In this study, we present a new regularization constraint to the existing l_1-norm regularized QSM reconstruction [6, 7]. The new regularization constraint incorporates prior information about the vessel anatomy and the orientation. The vessel orientation prior is estimated by extracting the vessel tree from QSM data using high order tensor vessel tractography [3].

2 Method

2.1 Segmentation

To extract a brain vessel tree from a given QSM image volume, we utilized a recent framework based on a higher order tensor vessel tractography by [8, 3]. The method in [3] involves a unified mathematical formulation which models the n-furcations, i.e. bifurcations or higher order junctions in vessel trees, jointly with tubular sections. A general Cartesian tensor is embedded into a 4-dimensional space so that antipodal asymmetries in Y-junction-like situations, which are abundant in vascular trees, can be accurately modeled. Starting from a few seed points (e.g. 5-6), an entire cerebral vein tree can be captured from the QSM by this technique, which provides the vessel orientation, its centerline (central lumen line), its thickness (vessel lumen diameter), locations of branching points, and lengths of branches. The extracted knowledge of centerlines permits OEF computation [9] along the vasculature. The only interaction to the method is providing seed points which lends itself to a simple practical vessel extraction process. The computation time for segmentation of the whole vessel tree is on the order of minutes (< 10 min).

2.2 l_1-regularized QSM reconstruction

To quantify oxygenation along brain vessels requires recovery of the underlying tissue susceptibility distribution from MRI observations of magnetic field perturbations. Tissue susceptibility χ is related to the measured field map ϕ via the formulation $\mathbf{DF}\chi = \mathbf{F}\phi$, where $\mathbf{F}$ is the Fourier transform operator and $\mathbf{D} = 1/3 - k_z^2/k^2$ is the susceptibility kernel in k-space. Due to the presence of zeros on the conical surface along the magic angle in this kernel, the solution of this system necessitates additional regularization.

Most popular types of existing QSM reconstruction techniques can be formulated by penalizing l_1-norm of gradients in three dimensions [7], and can be expressed as an unconstrained convex optimization problem, minimizing

$$\underset{\chi}{argmin}\ \frac{1}{2}\left\|\mathbf{F^{-1}DF}\chi - \phi\right\|_2^2 + \alpha \cdot \|\mathbf{G}\chi\|_1 \tag{1}$$

where α is the regularization parameter and $\mathbf{G} = [\mathbf{G_x}; \mathbf{G_y}; \mathbf{G_z}]$ is the gradient operator in three spatial directions.

2.3 l_1-regularized QSM reconstruction with vessel orientation (VO) constraint

We propose a new regularization term to be added to Eq. 1. As a regularizer, we use the dot product between the $\mathbf{G}\chi$ and the orientation vector $\mathbf{V} =$

$[\mathbf{V_x}; \mathbf{V_y}; \mathbf{V_z}] \in \mathbb{R}^{\mathbf{3}}$. The new regularization term incorporates prior information about the vessel anatomy and the orientation. We expect OEF (and thus susceptibility) along the vessel direction to be relatively smooth. Thus, the $\mathbf{G}\chi$ inside a vessel should be orthogonal to the $\mathbf{V}$, and the dot product between $\mathbf{G}\chi$ and $\mathbf{V}$ should be small. The final constraint is weighted by a dilated vessel mask $\mathbf{M}$: $\|\mathbf{M}(\mathbf{G} \cdot \mathbf{V})\chi\|_1$.

Hence, the l_1-regularized and vessel orientation constrained reconstruction problem reads as:

$$\underset{\chi}{argmin}\ \frac{1}{2}\left\|\mathbf{F^{-1}DF}\chi - \phi\right\|^2 + \alpha \cdot \|\mathbf{G}\chi\|_1 + \lambda \|\mathbf{M}(\mathbf{G} \cdot \mathbf{V})\chi\|_1 \tag{2}$$

where α and λ are the regularization parameters.

3 Experimental Results

In this section, we will show the results of the l_1-regularized QSM reconstruction with vessel orientation (VO) constraint on: (§ 3.1) a ground truth in vivo validation data; (§ 3.2) in vivo QSM volumes acquired on ten healthy volunteers; (§ 3.3) a single in vivo QSM volume registered with a contrast-enhanced Fast Spin Echo MRI (MFAST) data. The regularization parameters (α, λ) were determined by parameter sweeping based on the validation data. The values ($\alpha = 8.3 \cdot 10^{-4}$, $\lambda = 3.5 \cdot 10^{-2}$) that minimized the normalized root mean square error (RMSE) relative to the true χ were selected to be the optimal setting, and applied in all experiments.

3.1 Validation data

A ground truth in vivo QSM dataset is obtained using 3D-Gradient Echo (GRE) acquisition at 12 different head orientations relative to the main magnetic field. Since the dipole kernel $\mathbf{D}$ varies as a function of the angle between the subject's head and the main field, an overdetermined system can be formed using data from multiple orientations to mitigate the ill-conditioning of dipole inversion. This technique is termed Calculation Of Susceptibility through Multiple Orientation Sampling (COSMOS), and obviates the need for additional regularization [10] to provide ground-truth quality susceptibility maps. For this acquisition, a healthy volunteer (female, age 30) was scanned with a 32-channel head coil on a Siemens 3T Trio system using TR/TE = 35/25 ms at 1 mm isotropic resolution with BW = 100 Hz/pixel upon 15-fold acceleration with the Wave-CAIPI sequence [11]. Raw phase images were processed using Laplacian unwrapping [12] and SHARP background removal [13] to yield tissue phase images from each orientation, which were jointly inverted to provide the COSMOS χ solution. Using the COSMOS reconstruction as the ground truth χ map, the field map ϕ was simulated using the forward dipole model $\phi = \mathbf{F^{-1}DF}$, and Gaussian noise ($\sigma = 0.01$) was added.

Starting from the noisy field map, l_1-reconstruction results in 8.37% RMSE which is calculated in the whole volume. We segmented the vessel tree from the χ map using the higher order tensor based vessel extraction method described in § 2.1. Figure 1(a, c) depicts the extracted vessel tree with two levels of detail in segmentation. The results of less detailed (4 seed points are used) and

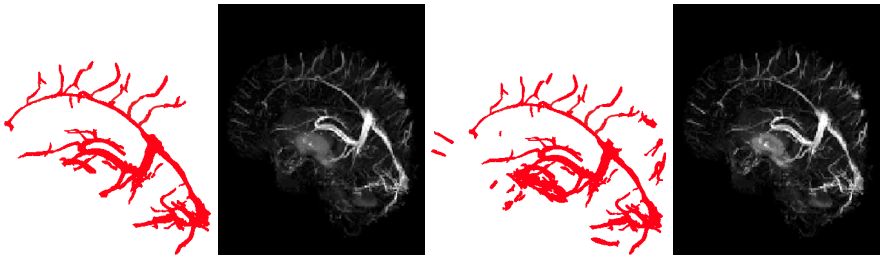

Fig. 1. A ground truth in vivo phantom data from QSM image with 12-orientations; (a) the less detailed vessel tree from the phantom data; (b) the result of l_1 regularized reconstruction with VO constraint for the less detailed vessel tree segmentation (4 seed points are used for vessel segmentation, and the reconstruction has 6.27% RMSE); (c) the more detailed vessel tree from the phantom data; (d) the result of l_1 regularized reconstruction with VO constraint for the more detailed vessel tree segmentation (7 seed points are used for vessel segmentation, and the reconstruction has 5.13% RMSE).

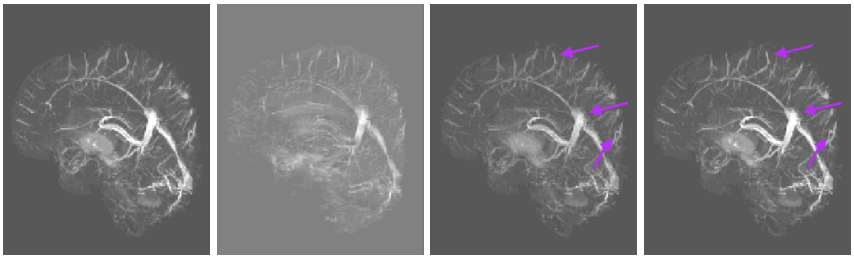

Fig. 2. Simulations result from ground truth susceptibility phantom. RMSE values were computed using a known ground truth susceptibility map. (a)Original χ field; (b) noisy normalized field map (input to QSM reconstruction); (c) l_1 regularized reconstructed χ field (8.37% RMSE); (d) l_1 regularized reconstructed with VO constraint χ field (5.13% RMSE). Arrows point out the reconstruction comparisons on the sample veins.

high detailed segmentation (7 seed points are used) are depicted in Figure 1(a) and Figure 1(c), respectively. l_1 regularized reconstruction with VO constraint has RMSE error of 6.27% with less detailed segmentation and 5.13% with more detailed segmentation (Figure 1(b) and Figure 1(d)). We observe that when the segmentation becomes more detailed, VO constraint is more effective in the reconstruction, thus RMSE decreases along the vessels. The results show that the improvement in the accuracy of the reconstruction with our vessel orientation constraint over the existing l_1 reconstruction is 40%. Qualitatively, it can be observed that smaller vessels are more visible in the reconstructions regularized with the additional VO constraint (Figure 2).

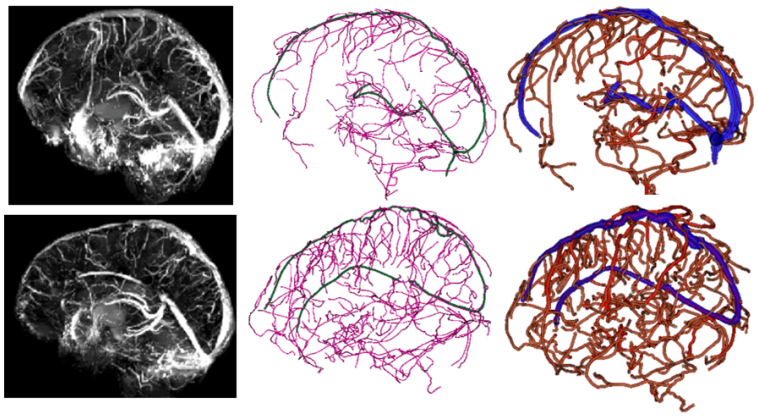

Fig. 3. (Right Column) Original QSM map; (Middle Column) extracted centerlines of the vessels; (Left Column) surface renderings for the vessels are shown for two healthy subjects.

3.2 In vivo MRI data

Ten young, healthy volunteers were scanned with a 32-channel coil on a Siemens 3T Trio system. 3D-GRE images for susceptibility mapping were acquired with full flow-compensation along each axis at all echoes. Axial magnitude and phase images were collected with TR = $23ms$; TE = $7.2/17.7ms$; resolution = $0.875 \times 0.875 \times 1mm^3$, matrix = $226 \times 256 \times 144$; and BW = 260Hz/pixel. Phase images were combined offline and processed with Laplacian unwrapping [12]. Background field was removed with SHARP filtering [13] and QSM reconstruction was performed with a l_1 regularized reconstruction technique [6].

Figure 3 depicts the QSM map, centerlines and surfaces of the vessel trees on two healthy volumes. We compute the OEF values [9] after the l_1 regularized reconstruction with and without VO constraint on the same subjects. Mean OEF of l_1 regularized reconstruction result across all veins are $33.3 \pm 4\%$, $35.7 \pm 7\%$, $31.7 \pm 3\%$, $38.6 \pm 5\%$, $37.4 \pm 6\%$, $33.8 \pm 3\%$, $33.7 \pm 2\%$, $35.7 \pm 5\%$, $31.9 \pm 4\%$, and $34.3 \pm 9\%$ respectively, for each of ten subjects. Estimated OEF for straight sinus, sagittal sinus, pial vessels are $46.3 \pm 6\%$, $36.4 \pm 4\%$, $31.8 \pm 3\%$, respectively, in average of ten subjects. Furthermore, we display the OEF values on the vessel surfaces of the sample two subjects, where the VO constraint is shown to improve conspicuity of smaller vessels (Figure 4).

3.3 QSM + MFAST data

With IRB approval, patients were scanned on a 3T GE scanner (MR750, GE Healthcare Systems, Waukesha, WI) with an 8-channel head-coil. A flow-compensated 3D parallel-imaging-accelerated multi-echo (ME)-GRE sequence was used with the following parameters: Axial plane, FOV = $22cm$, matrix size = 384×256, number of partitions = 66, resolution = $0.6 \times 0.9 \times 2mm^3$, acceleration factor = 2, flip angle = 15°, TR = 36ms, seven echoes ranging from TE = $4ms - 33ms$ ($4.8ms$ increments), scan time = $5.44min$. On completion of the scan, the raw

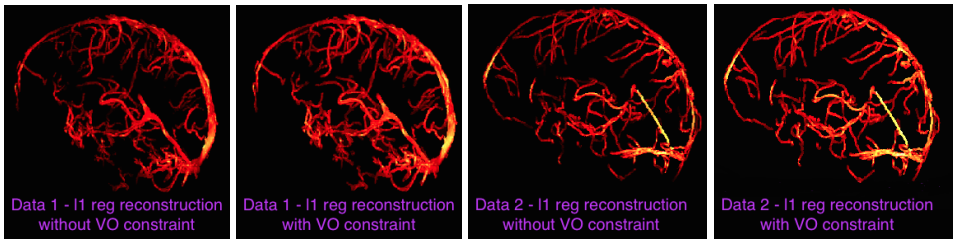

Fig. 4. OEF visualization on two sample subjects from ten data volume (shown in hot colors); (a) QSM reconstruction without vessel orientation is shown on the first subject; (b) the result of l_1 regularized reconstruction with VO constraint is shown on the first subject; (c) QSM reconstruction without vessel orientation is shown on the second subject; (d) the result of l_1 regularized reconstruction with VO constraint is shown on the second subject.

data from the scanner were automatically reconstructed using compiled threaded MATLAB (MathWorks Inc., Natick, MA, USA) code.

A ferumoxytol-enhanced MRA using 3D SPGR was designed with short repetition time (TR) = 4ms and echo time (TE) = 1 ms. The sequence was fat suppressed with FOV = $26cm$, matrix size = 416×416, resolution = $0.625\times0.625mm^2$ and 180 slices with 1 mm thickness. The excitation was done with a flip angle of 15 degrees, and receiver bandwidth of $62.5kHz$. The scan time was reduced by not acquiring the corners of ky-kz space, producing an acquisition time of $5.46min$.

We first extracted the brain using FSL [14] from MFAST data, then registered MFAST and QSM data with a rigid registration using the MedInria software [15]. Using the QSM reconstruction as the reference χ map, the field map ϕ was simulated using the forward dipole model, and Gaussian noise was added ($\sigma = 0.02$). Then, we segmented the vessel tree from QSM data and MFAST data separately. Figure 5 (Top row) shows the vessel tree segmentation from QSM and MFAST data, respectively. We use morphological operators to separate veins from arteries for the MFAST data. Figure 5 (Bottom row) visualizes the results of: (First column) QSM reconstruction without the vessel orientation prior; (Second column) QSM reconstruction with the vessel orientation prior where the vessel tree is segmented from the QSM data; (Third column) QSM reconstruction with the vessel orientation prior where the vessel tree is segmented from the MFAST data. The results show the enhancements along the veins using our VO prior in the reconstructions. The amount of detail captured in the vessel tree extracted from the MFAST data volume, which is then incorporated into the QSM reconstruction through the VO regularizer clearly reveals the benefits of the new regularizer term.

4 Conclusion

We developed a method that improves the accuracy of l_1 regularized QSM reconstruction [6, 7] with a new regularization constraint, vessel orientation. Quantita-

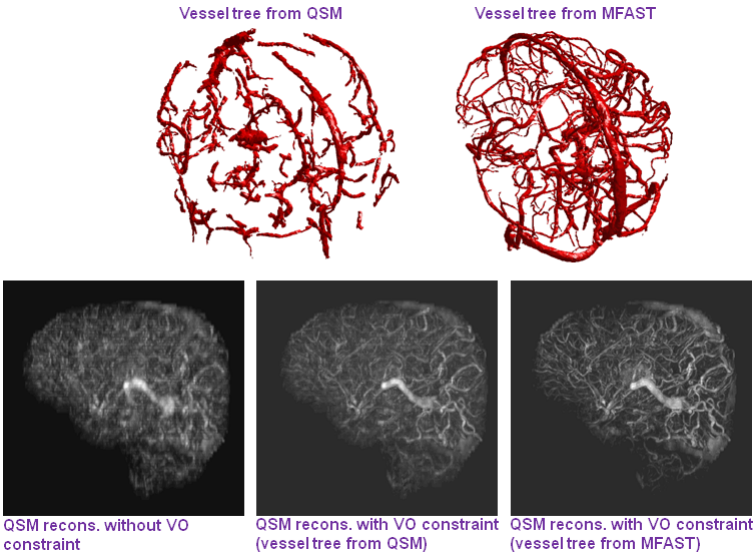

Fig. 5. Top row: Left Column-Vessel tree extraction from QSM data, Right Column-vessel tree extraction from MFAST data ; Bottom row: (First column) QSM reconstruction without vessel orientation, (Second column) l_1-reg QSM data reconstructed with vessel orientation constraint (Vessel tree is extracted from the QSM data), (Third column) l_1-reg QSM data reconstructed with vessel orientation constraint (Vessel tree is extracted from the MFAST data).

tive performance of our method was demonstrated on a ground truth phantom data. Furthermore, we performed the experiments on ten QSM images reconstructed from MRI phase and presented the mean OEF results for all veins in each volume and major vessel segments. On two sample subjects, we showed that the OEF maps along the vessel direction are relatively smooth. Finally, we compared the QSM reconstructions on a QSM volume acquired with an additional modality, the MFAST. We showed the results for QSM reconstructions with and without vessel orientations where the vessel trees were segmented from QSM and MFAST data respectively. Use of the vessel orientation constraint increased OEF values (Figure 4), such that our results are more in line with physiological OEF values reported by O-15 PET imaging [16]. This observation suggests that the use of anatomical prior helps mitigate partial volume effects and over-smoothing associated with traditional regularized QSM reconstruction.

References

1. Wycliffe, N.D., Choe, J., Holshouser, B., Oyoyo, U.E., Haacke, E.M., Kido, D.K.: Reliability in detection of hemorrhage in acute stroke by a new three-dimensional gradient recalled echo susceptibility-weighted imaging technique compared to computed tomography: A retrospective study. Journal of Magnetic Resonance Imaging **20**(3) (2004) 372–377

2. Hammond, K.E., Lupo, J.M., Xu, D., Veeraraghavan, S., Lee, H., Kincaid, A., Vigneron, D.B., Manley, G.T., Nelson, S.J., Mukherjee, P.: Microbleed detection in traumatic brain injury at 3t and 7t: Comparing 2d and 3d gradient-recalled echo (gre) imaging with susceptibility-weighted imaging (swi). ISMRM **248** (2009)
3. Cetin, S., Unal, G.: A higher-order tensor vessel tractography for segmentation of vascular structures. Medical Imaging, IEEE Transactions on **34**(10) (Oct 2015) 2172–2185
4. Serres, B., Deistung, A., Schfer, A., Kocinski, M., Materka, A., Reichenbach, J.: Automatic segmentation of the venous vessel network based on quantitative susceptibility maps and its application to investigate blood oxygenation. ISMRM **169** (2015)
5. Christen, T., Bolar, D.S., Zaharchuk, G.: Imaging Brain Oxygenation with MRI Using Blood Oxygenation Approaches: Methods, Validation, and Clinical Applications. American Journal of Neuroradiology (August 2012)
6. Bilgic, B., Fan, A.P., Polimeni, J.R., Cauley, S.F., Bianciardi, M., Adalsteinsson, E., Wald, L.L., Setsompop, K.: Fast quantitative susceptibility mapping with l1-regularization and automatic parameter selection. Magnetic Resonance in Medicine **72**(5) (2014) 1444–1459
7. de Rochefort, L., Liu, T., Kressler, B., Liu, J., Spincemaille, P., Lebon, V., Wu, J., Wang, Y.: Quantitative susceptibility map reconstruction from mr phase data using bayesian regularization: Validation and application to brain imaging. Magnetic Resonance in Medicine **63**(1) (2010) 194–206
8. Cetin, S., Demir, A., Yezzi, A.J., Degertekin, M., Unal, G.: Vessel tractography using an intensity based tensor model with branch detection. IEEE Trans. Med. Imaging **32**(2) (2013) 348–363
9. Fan, A.P., Bilgic, B., Gagnon, L., Witzel, T., Bhat, H., Rosen, B.R., Adalsteinsson, E.: Quantitative oxygenation venography from mri phase. Magnetic Resonance in Medicine **72**(1) (2014) 149–159
10. Liu, T., Spincemaille, P., de Rochefort, L., Kressler, B., Wang, Y.: Calculation of susceptibility through multiple orientation sampling (cosmos): A method for conditioning the inverse problem from measured magnetic field map to susceptibility source image in mri. Magnetic Resonance in Medicine **61**(1) (2009) 196–204
11. Bilgic, B., Xie, L., Dibb, R., Langkammer, C., Mutluay, A., Ye, H., Polimeni, J.R., Augustinack, J., Liu, C., Wald, L.L., Setsompop, K.: Rapid multi-orientation quantitative susceptibility mapping. NeuroImage **125** (2016) 1131 – 1141
12. Li, W., Wu, B., Liu, C.: Quantitative susceptibility mapping of human brain reflects spatial variation in tissue composition. NeuroImage **55**(4) (2011) 1645 – 1656
13. Schweser, F., Deistung, A., Lehr, B.W., Reichenbach, J.R.: Quantitative imaging of intrinsic magnetic tissue properties using {MRI} signal phase: An approach to in vivo brain iron metabolism? NeuroImage **54**(4) (2011) 2789 – 2807
14. Smith, S.M.: Fast robust automated brain extraction. Human Brain Mapping **17**(3) (2002) 143–155
15. Toussaint, N., christophe Souplet, J., Fillard, P.: Medinria: medical image navigation and research tool by inria. In: In: Proceedings of MICCAI Workshop on Interaction in Medical Image Analysis and Visualization. (2007)
16. Bremmer, J.P., Berckel, B.N.M., Persoon, S., Kappelle, L.J., Lammertsma, A.A., Kloet, R., Luurtsema, G., Rijbroek, A., Klijn, C.J.M., Boellaard, R.: Day-to-day test–retest variability of cbf, cmro2, and oef measurements using dynamic 15o pet studies. Molecular Imaging and Biology **13**(4) (2010) 759–768